Tuning cross-linker type in the fabrication of beta-cyclodextrin/magnetic lignin adsorbents: Comparative study of cationic dye adsorption performance

Arefe Moatamed Sabzevar [a,b], Ali Ahmadpour [a,b,*],
Mahboube Ghahramaninezhad [a,b], Arash Arami-Niya [c,**]

[a] Department of Chemical Engineering, Faculty of Engineering, Ferdowsi University of Mashhad, PO Box 91779-48944, Mashhad, Iran
[b] Industrial Catalysts, Adsorbents, and Environment Lab., Oil and Gas Research Institute, Ferdowsi University of Mashhad, PO Box 91779-48974, Mashhad, Iran
[c] Discipline of Chemical Engineering, Western Australian School of Mines: Minerals, Energy and Chemical Engineering, Curtin University, GPO Box U1987, Perth, WA 6845, Australia

ABSTRACT

This study investigates the use of three specific carboxylic acids, citric acid (CA), malic acid (MA), and tartaric acid (TA), as cross-linkers to develop adsorbents for water treatment that integrate the distinctive characteristics of magnetic kraft lignin (MKL) and beta-cyclodextrin (β-CD), thereby achieving improved efficiency and stability. The adsorbents were synthesized via the esterification method and characterized using various analytical techniques, including X-ray diffraction (XRD), Fourier transform infrared spectroscopy (FTIR), field-emission scanning electron microscopy (FESEM), and a vibrating sample magnetometer (VSM). Response surface methodology (RSM) was used to design experiments and optimize conditions to achieve the optimal parameters of pH, contact time, and solid-to-solution ratio (dose) in the removal of methylene blue. The results indicated that methylene blue removal could reach approximately 97% under optimal conditions: pH 11, a contact time of 30 min, and a dose of 0.2 $g.L^{-1}$. The Langmuir model provided the best fit for the equilibrium data, with a maximum adsorption capacity of 454.54 $mg.g^{-1}$. Kinetic analysis revealed that the sorption process adhered to a pseudo-second-order model. The obtained results highlight the excellent potential of β-CD-TA-MKL as an efficient and sustainable adsorbent for the removal of methylene blue. Notable advantages of β-CD-TA-MKL compared to other reported adsorbents include its higher adsorption capacity, remarkable stability over five regeneration cycles with minimal loss in performance, rapid adsorption kinetics, and the utilization of environmentally friendly, cost-effective materials.

1. Introduction

Water pollution is a global issue due to elevated levels of aromatic pollutants, which are complex and poorly biodegradable

---

* Corresponding author at: Department of Chemical Engineering, Faculty of Engineering, Ferdowsi University of Mashhad, PO Box 91779-48944, Mashhad, Iran.
** Corresponding author.
E-mail addresses: ahmadpour@um.ac.ir (A. Ahmadpour), arash.araminiya@curtin.edu.au (A. Arami-Niya).

compounds released from industries such as dyeing (Zuhara et al., 2023), textiles, paper, cosmetics, and leather (Shindhal et al., 2021). Among these, methylene blue (MB), a phenothiazine salt, remains relatively stable in alkaline aqueous solutions and significantly reduces water clarity (Sun et al., 2021). The adsorption technique is widely used for efficient water purification because of its affordability (Yatimzade et al., 2024), simplicity of operation, and enhanced efficiency (Chahal et al., 2024). Numerous adsorbents, including activated carbon, nanofibers, and graphene oxide, are utilized in adsorption processes. However, many of these materials face challenges, including non-biodegradability, high costs (Zong et al., 2018), complex synthesis, and challenging separation (Zhong et al., 2022). These limitations underscore the growing need for cost-effective adsorbents with high adsorption capacity and rapid adsorption equilibrium times (Zong et al., 2018).

Growing environmental concerns and the depletion of fossil resources have increased interest in natural biomass-derived materials, including cellulose, chitosan, and lignin (Wu et al., 2021). Lignin, an aromatic macromolecule and byproduct of papermaking and polysaccharide-based biorefineries (Li et al., 2021), is particularly promising. Its abundance of hydroxyl groups enables chemical modification (Zhang et al., 2023), but its complex, amorphous structure and strong inter- and intramolecular hydrogen bonding often lead to aggregation, reducing adsorption efficiency. Fortunately, structural modifications such as grafting, cross-linking, polymerization, or substitution with active groups can enhance its properties for specific applications (Wu et al., 2021).

Beta-cyclodextrin (β-CD), a macrocyclic oligosaccharide characterized by a hydrophobic inner cavity and a hydrophilic outer surface (Ghahramaninezhad and Ahmadpour, 2022), has attracted significant attention for pollutant treatment (Zhong et al., 2022) due to its low cost, biodegradability, and environmental compatibility. However, its water solubility poses challenges for separation and collection in practical applications. This limitation is often addressed through cross-linking or immobilization (Liu et al., 2022). Rohith and Girija designed a multifunctional polymeric adsorbent using β-CD and Nelumbo nucifera agricultural waste, demonstrating its high removal efficiency for toxic dyes with excellent stability (Rohith and Girija, 2024). Similarly, Qu et al. reported graphene oxide/β-CD composites with high MB adsorption and excellent reusability (Qu et al., 2025).

Magnetic adsorbents based on lignin and β-CD have gained attention because external magnetic fields enable efficient separation from aqueous systems. Magnetite (Fe_3O_4), widely used for its biocompatibility, environmental stability, and strong magnetic properties, enhances the practicality of such composites. For example, lignin@Fe_3O_4 nanocomposites achieved 55.6% MB removal at a lignin-to-Fe_3O_4 mass ratio of 1:1, which increased to 74.1% at a 20:1 ratio (Petrie et al., 2021). Similarly, Liu et al. synthesized porous magnetic β-CD polymer nanospheres with a maximum MB adsorption capacity of 305.8 mg.g^{-1}, outperforming β-CD-modified Fe_3O_4 nanoparticles (Liu et al., 2019). More recently, Liu et al. developed composites incorporating aminated Fe_3O_4, graphene oxide, and carboxylated cross-linked β-CD polymer, achieving an adsorption capacity of 201.7 mg.g^{-1} (Liu et al., 2024).

The complementary properties of lignin and β-CD, functional groups for diverse interactions and host–guest complexation, respectively, make their combination in magnetic composites particularly promising. Yet, the development of environmentally friendly magnetic lignin–β-CD adsorbents using bio-based cross-linkers remains underexplored. Carboxylic acids, including di- and polycarboxylic acids, are attractive cross-linkers due to their multiple strong reactive sites, enabling stable cross-linking networks through esterification and intermolecular bonding (Castro and Santana, 2024). In our earlier work, we used citric acid (CA) as a green cross-linker to attach β-CD to magnetic kraft lignin (MKL), offering a safer alternative to epichlorohydrin (Sabzevar et al., 2024). Although the resulting adsorbent showed good reusability and efficient MB removal, its adsorption capacity was limited, likely due to steric hindrance from CA reducing access to active sites (Altayan et al., 2023).

To address this limitation, the present study investigates malic acid (MA) and tartaric acid (TA) as alternative bio-based cross-linkers with improved molecular symmetry and reduced steric hindrance compared to CA. These characteristics are expected to enhance cross-linking, improve the polymer network between β-CD and MKL, and boost adsorption capacity. Accordingly, β-CD-MA-MKL and β-CD-TA-MKL adsorbents were synthesized and tested for MB removal. In these composites, β-CD facilitates host–guest inclusion complexation, the cross-linkers enhance electrostatic interactions, and MKL provides a functional structural backbone. The magnetic properties allow for rapid, easy recovery without filtration or centrifugation.

Using Design-Expert software, batch adsorption experiments were performed to study the effects of pH, adsorbent dose, and contact time. To the best of our knowledge, this is the first study to modify magnetic lignin with β-CD using MA and TA as cross-linkers. The results demonstrate significantly improved adsorption capacity, highlighting the potential of bio-based, renewable cross-linkers to enhance green adsorbent design while reducing reliance on toxic or costly materials.

2. Experimental section

2.1. Materials and reagents

Kraft lignin (molecular weight ∼ 10,000 g mol^{-1}) and beta-cyclodextrin (≥ 97%) were sourced from Sigma-Aldrich. Iron (Fe^{3+}) chloride hexahydrate, iron (Fe^{2+}) sulfate heptahydrate, ammonia solution (28 wt%), potassium dihydrogen phosphate (KH_2PO_4), CA, MA, TA, hydrochloric acid (HCl, 37 wt%), sodium hydroxide (NaOH), sodium chloride (NaCl), MB, methyl orange (MO), rhodamine B (RB), crystal violet (CV) and absolute ethanol (CH_3CH_2OH) were sourced from Merck. Table S1 displays the properties of the cross-linkers examined in this work.

2.2. Synthesis of cross-linked β-CD on MKL using carboxylic acids

The preparation procedure of the adsorbents is illustrated in Scheme 1. The synthesis method was performed based on our previously published work (Sabzevar et al., 2024). Further details on the MKL synthesis method are provided in Section S-1 of the

Supporting Information (SI). The esterification protocol used in this study was developed based on methods reported in previous articles (Jemli et al., 2024; Jiang et al., 2021; Silva et al., 2024), with the difference that the amounts of starting materials were adjusted to optimize for our experimental conditions, and changes were made to the reaction time and type of cross-linkers used.

For the preparation of each of the adsorbents, MKL (0.1 g), β-CD (0.4 g, 0.35 mmol), 0.4 g of the respective cross-linker (CA or MA or TA), and KH_2PO_4 (0.24 g, 1.7 mmol) with 15 mL of Deionized (DI) water were mixed in a beaker and stirred for 2 h. Then, the mixture was added to a Petri dish and heated at 140°C for 2 h in an oven. After cooling, the resulting crude product was repeatedly soaked in water and rinsed three to four times with deionized water, then filtered with a magnet and dried under vacuum at 60°C overnight. The synthesized adsorbents were named according to the type of carboxylic acid used as the cross-linker for magnetic kraft lignin (MKL) and beta-cyclodextrin (β-CD). Specifically, the adsorbents synthesized with citric acid (CA), malic acid (MA), and tartaric acid (TA) were labeled as β-CD-CA-MKL, β-CD-MA-MKL, and β-CD-TA-MKL, respectively. They should be stored in a closed container at room temperature until use and subsequent characterization.

2.3. Characterization of the adsorbents

Several analytical techniques were used to characterize the synthesized adsorbents. The crystal structures of adsorbents were studied by X-ray diffraction analysis (XRD, GNR Explorer X-ray diffractometer, Italy) in the range of 2θ from 5 to 70°. The functional groups were identified via Fourier transform infrared spectroscopy (FTIR, Thermo Nicolet Avatar 370 spectrometer, USA) in the range of 400–4000 cm^{-1}. The morphologies of the adsorbents were observed using a field-emission scanning electron microscope (FESEM, Tescan Mira III LMU, Czech Republic) coupled with energy-dispersive X-ray spectroscopy (EDS) to identify elements. Before imaging, each adsorbent was coated with a thin layer of gold to enhance resolution.

Using a Zeta analyzer (CAD Zeta Compact, France), the surface charge of adsorbents was determined at different pH values. The adsorption behavior of the pollutant was evaluated using UV–visible spectroscopy (Analytic Jena-Spekol 1300, Germany) at a wavelength of λ_{max} = 664 nm. The magnetic properties of the adsorbents were measured using a vibrating sample magnetometer (VSM, Magnetic Danesh Pajoh Inst., Iran). The chemical composition and elemental distribution on the surface of the adsorbents were determined using X-ray photoelectron spectroscopy (XPS) measurements (Bes Tec, Germany) with Al K-α radiation (1486.6 eV).

2.4. Batch adsorption study

The batch adsorption experiments were performed using the response surface methodology (RSM) in Design-Expert software (Version 13.0.15) to investigate the adsorbent's ability to remove MB. A more complete description of the adsorption experiments, the applied equations (Eqs. (S1) and (S2)), and the empirical second-order polynomial model (Eq. (S3)) in Section S-2, as well as the techniques used to identify β-CD (Section S-3) and its equation (Eq. (S4)), are provided in the SI.

The RSM, based on the central composite design (CCD), was utilized to investigate the effect of three independent variables of pH (3−11), adsorbent dose (0.2−0.6 g.L^{-1}), and contact time (10−30 min) on the removal of MB. This approach, one of the common mathematical and statistical design methods, is used to evaluate the effects of the variables under study on the response surface by carefully assessing deviations in the experiment and reducing the systematic errors in the process (Kumari et al., 2023b). Also, it requires fewer experiments compared to the traditional one-factor-at-a-time (OFAT) approach, revealing complex interactions more
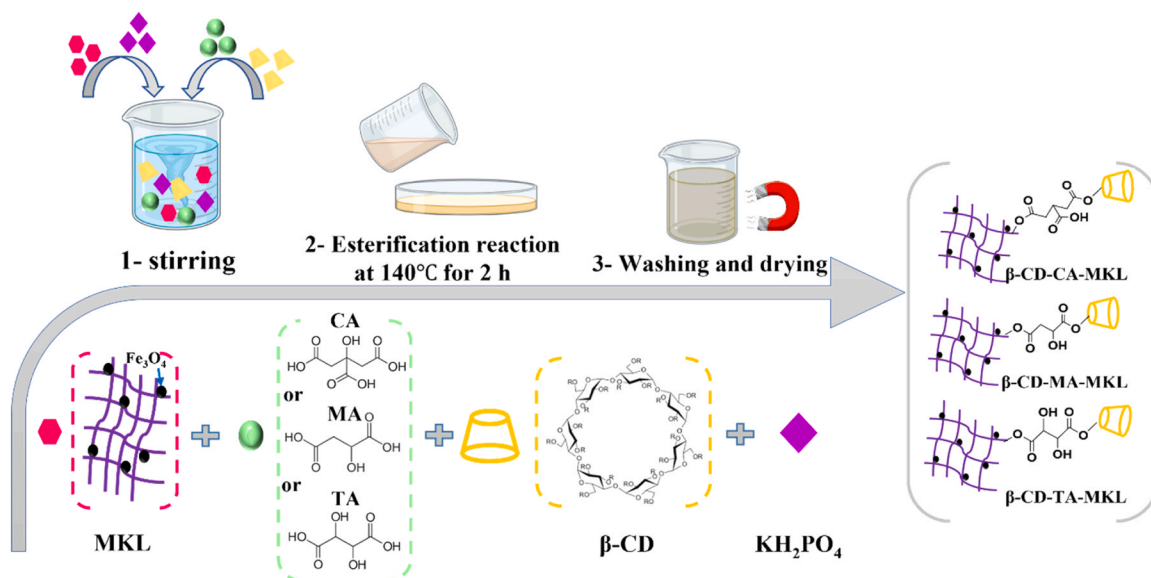
Scheme 1. Preparation procedure of adsorbents and schematic of the potential reaction mechanism.

effectively (Reza et al., 2024). While the Taguchi method can optimize parameters, it mainly focuses on linear interactions. It provides only one optimal value, making it slightly less accurate than RSM, which examines all parameter combinations and uses a utility function to guide experiments (Tan et al., 2017). Other methods like Genetic Algorithms, Artificial Neural Networks (ANNs), and Particle Swarm Optimization have their advantages and limitations, such as computational cost, difficulty in interpretation, and sensitivity to initial conditions, respectively (Kumari et al., 2023b).

RSM, combined with CCD, is widely used in water treatment applications, but it has limitations when describing behaviors beyond linear or quadratic relationships. Machine learning approaches such as ANNs perform better in nonlinear systems, but they require large datasets, high computational power, and can obscure process understanding. RSM is computationally efficient and interpretable, although sensitive to noise (Kumari et al., 2025). Kumari et al. showed that both ANN and RSM models predicted high adsorption efficiencies of MB, reaching up to 94.6 % and 93.2 %, respectively, indicating the effectiveness of Juglans regia as an adsorbent (Kumari et al., 2025). Studies show RSM effectively predicts high MB adsorption efficiency (Obayomi et al., 2024). Given that the developed model in this study is quadratic, RSM was selected for its accuracy, ability to optimize multiple variables simultaneously, and proven applicability in similar research (Obayomi et al., 2024).

As shown in Table S2, operational parameters were examined at five levels ($-\alpha$, -1, 0, $+1$, $+\alpha$). A design with three factors and five levels comprising 34 experiments was created to optimize the adsorption of MB dye.

2.5. Statistical evaluation

Quantitative data are presented as mean $\pm$ standard deviation or standard error of the mean. A one-way analysis of variance (ANOVA) was conducted for each time point in the data shown in Fig. 1 to determine if the four adsorbents (MKL, β-CD-CA-MKL, β-CD-MA-MKL, and β-CD-TA-MKL) had statistically significant variations in MB removal efficiency. For each adsorbent and at each time point, experiments were performed in triplicate (n = 3). The experimental design was developed using Design-Expert software based on the generated matrix. Each run was conducted in duplicate, except for the center point, which was repeated six times to estimate the experimental error. For the statistical evaluation, Eqs. (S5-S8) in Section S-4 were used to determine the model's goodness of fit to the experimental data.

3. Results and discussion

3.1. Optimization of key parameters in adsorbent synthesis

Although CA was used as a cross-linker in our previous study (Sabzevar et al., 2024), detailed optimization of synthesis parameters, including temperature, reaction time, and amounts of CA and KH_2PO_4, is reported here for the first time. Other adsorbents were synthesized using the optimized conditions established for β-CD-CA-MKL. The condensation reaction between the carboxyl groups of CA and the hydroxyl groups of MKL and β-CD is widely known to be significantly affected by the reaction temperature. Fig. S1(a) illustrates the role of reaction temperature on the MB adsorption capacity. Increasing the reaction temperature (80–140°C) under specific conditions (0.4 g of β-CD, 0.4 g of CA, 0.1 g of MKL, 0.24 g of KH_2PO_4, and a reaction time of 2 h) directly correlates with an increase in MB adsorption capacity. This enhancement can be associated with (1) the increased emission rate of CA molecules in the vicinity of β-CD and MKL molecules, (2) the higher condensation efficiency (El-Tahlawy et al., 2006), and greater β-CD grafting onto MKL. Our results indicate the optimal reaction temperature is 140°C, as the adsorbent prepared at this temperature exhibits the highest adsorption capacity. Further increases in temperature up to 160°C result in a reduction in adsorption capacity due to the degradation of CA into unsaturated acids and anhydrides (Ghorpade et al., 2016). Consequently, β-CD cannot attach to the MKL and is removed as an
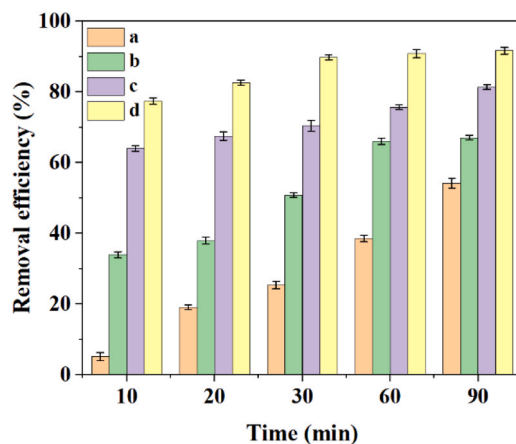

Fig. 1. Comparison of removal efficiency using (a) MKL, (b) β-CD-CA-MKL, (c) β-CD-MA-MKL, and (d) β-CD-TA-MKL (MB concentration: 20 mg.L^{-1} and adsorbent dose: 0.2 g.L^{-1}).

ester during the washing process (Ghorpade et al., 2016). These findings align with those reported by Silva et al., who also identified 140°C as the optimal esterification temperature (Silva et al., 2024). The relationship between the duration of the esterification reaction and the adsorption capacity of the adsorbent is illustrated in Fig. S1(b). Esterification was conducted with 0.4 g of β-CD, 0.4 g of CA, 0.1 g of MKL, and 0.24 g of KH_2PO_4 at 140°C. The results demonstrate that increasing reaction time enhances the esterification process. A reaction time of 2 h is optimal, as extending the duration to 3 h does not lead to significant changes in adsorption capacity.

Fig. S1(c) shows the effect of KH_2PO_4 amount (0–0.48 g) as a catalyst in the esterification process (under the conditions of 0.4 g of β-CD, 0.4 g of CA, 0.1 g of MKL, reaction time: 2 h at 140°C). Increasing the KH_2PO_4 amount from 0 to 0.24 g enhances the carboxyl content and facilitates β-CD grafting onto MKL via CA, thereby improving the adsorption capacity. However, further increases in KH_2PO_4 amount (0.24–0.48 g) lead to a dilution effect, where the catalyst acts as a barrier between β-CD and CA, hindering their interaction. This trend is similar to the effect reported for sodium hypophosphite catalyst (Ghorpade et al., 2016). Thus, a KH_2PO_4 amount of 0.24 g is optimal for MB removal. The influence of CA amount (0–0.8 g) on the extent of esterification and adsorption capacity is depicted in Fig. S1(d). The reaction, conducted with 0.4 g of β-CD, 0.1 g of MKL, and 0.24 g of KH_2PO_4 at 140°C for 2 h, shows that increasing the CA amount enhances the carboxyl content and adsorption capacity. This is due to the greater availability of CA molecules (El-Tahlawy et al., 2006) near the β-CD and MKL molecules at higher amounts, which enhances the extent of esterification, consistent with the trend reported (El-Tahlawy et al., 2006). Therefore, the optimal condition for preparing β-CD-CA-MKL is 0.4 g of CA.

After optimizing the preparation conditions for β-CD-CA-MKL, the same synthesis protocol was applied to produce β-CD-MA-MKL and β-CD-TA-MKL. The impact of cross-linker types on the removal efficiency of MB was then investigated. As shown in Fig. 1, the adsorption of MB by the adsorbents gradually increases from 10 to 90 min. Among the adsorbents, β-CD-TA-MKL exhibits the highest increase in removal efficiency. This improvement can be attributed to the symmetrical arrangement of OH groups and the reduced steric hindrance in the TA cross-linker's structure, compared to those of MA and CA cross-linkers, which facilitates more effective access of dye molecules to the active sites of the adsorbent by reducing steric barriers. According to Table S3, the levels of active β-CD follow the trend: β-CD-TA-MKL> β-CD-MA-MKL> β-CD-CA-MKL.

Due to the greater tendency of β-CD-TA-MKL adsorbent to remove MB, subsequent adsorption tests were conducted using this adsorbent. The p-values for the percentage of MB removal at time intervals of 10, 20, 30, 60, and 90 min were 2.34×10^{-6}, 5.93×10^{-6}, 0.0012, 4.38×10^{-5}, and 3.88×10^{-5}, respectively. All values are less than 0.05, indicating statistically significant
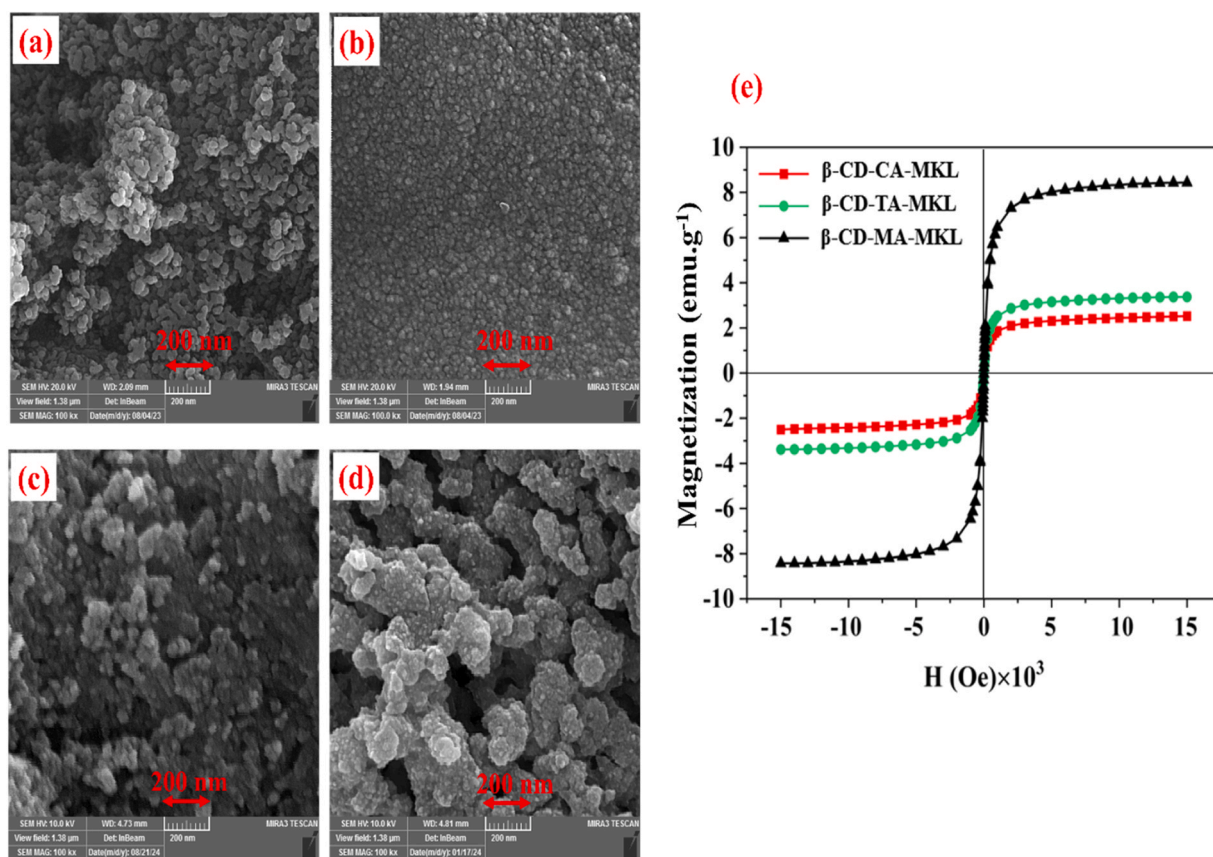

Fig. 2. FESEM images of (a) MKL, (b) β-CD-CA-MKL, (c) β-CD-MA-MKL, and (d) β-CD-TA-MKL; (e) magnetic hysteresis loop of the synthesized adsorbents.

differences (Kwak, 2023).

3.2. Characterization of the adsorbents

It is worth noting that the characterization data of the MKL and β-CD-CA-MKL adsorbents presented in this study were adopted from our previous work (Sabzevar et al., 2024), as the structures and composition remained unchanged. These data were included alongside the newly synthesized adsorbents (β-CD-MA-MKL and β-CD-TA-MKL) for comparative purposes only.

XRD analysis was performed to compare the structural information of β-CD-CA-MKL (Sabzevar et al., 2024), β-CD-MA-MKL, and β-CD-TA-MKL, as shown in Fig. S2. The peaks at 30.25°, 35.66°, 43.78°, 57.31°, and 63.07° confirm the presence of the Fe_3O_4 phase (Petrie et al., 2021) in β-CD-MA-MKL and β-CD-TA-MKL adsorbents, which show a face-centered cubic (FCC) structure. These peaks were also present in the synthesized MKL in our previous work (Sabzevar et al., 2024) before modification, indicating that the crystalline structure of iron remained unchanged after cross-linking in adsorbents, and only the intensity and width of the peaks changed. A comparison of the diffraction patterns of the β-CD-CA-MKL (Sabzevar et al., 2024), β-CD-MA-MKL, and β-CD-TA-MKL shows that the peaks of the β-CD-CA-MKL adsorbent (Sabzevar et al., 2024) are weaker and broader than the other two. Thus, it indicates smaller crystals (Wang et al., 2014). In contrast, the β-CD-MA-MKL adsorbent shows larger crystals with sharp peaks and higher intensities. These changes claim that the type of cross-linker is important in the crystal growth process. The Scherrer equation (Eq. (S9) in Section S-5) (Petrie et al., 2021) was used to determine the crystallite sizes of β-CD-CA-MKL (Sabzevar et al., 2024), β-CD-MA-MKL, and β-CD-TA-MKL based on their XRD patterns. The estimated crystallite sizes were 4.11, 10.72, and 8.60 nm, respectively.

The FTIR is commonly employed to identify ester groups in biomaterials cross-linked with carboxylic acids (Altayan et al., 2023). The FTIR spectra of β-CD-CA-MKL (Sabzevar et al., 2024), β-CD-MA-MKL, and β-CD-TA-MKL, as presented in Fig. S3 and Table S4, exhibit similar peak positions, suggesting that the functional groups introduced by the different cross-linkers are largely the same. In contrast, the spectra of the adsorbents differ significantly from that of MKL (Sabzevar et al., 2024), indicating that surface modification with β-CD via the cross-linkers was successful. As shown in Fig. S3, new absorption bands at 1742 cm^{-1} and 1747 cm^{-1} in β-CD-MA-MKL and β-CD-TA-MKL, respectively, are related to the C=O stretching vibration of the ester group. This indicates that the esterification reaction has been completed (Zhou et al., 2018), and the carboxylic acid groups of the cross-linking agent have formed ester bonds with the –OH groups of β-CD and MKL. The similarity among β-CD-CA-MKL (Sabzevar et al., 2024), β-CD-MA-MKL, and β-CD-TA-MKL further suggests that the choice of cross-linker does not introduce unique or additional functional groups.

Based on FESEM images, the MKL particles (Sabzevar et al., 2024) in Fig. 2(a) display a spherical shape, which is in agreement with similar findings (Cao et al., 2023). Grafting of β-CD (Fig. 2(b), (c), (d)) alters the size of particles, but the morphology remains visually unchanged. We suggest that this difference in particle size is likely attributed to variations in the structure of the cross-linkers used in adsorbent synthesis. CA, with its three carboxylic groups and ability to form denser cross-links, likely promotes the formation of a more compact and denser network structure (Pooja et al., 2025). This may lead to smaller particle sizes. Zhou et al. reported that the size of starch nanocrystals decreased after cross-linking modification with CA (Zhou et al., 2016). In contrast, MA and TA with fewer functional groups may form less dense networks or localized clusters, leading to larger particle sizes. The EDS spectrum for β-CD-TA-MKL and β-CD-MA-MKL (Table S5) reveals the presence of iron, carbon, oxygen, and sulfur in the adsorbents. For β-CD-CA-MKL (Sabzevar et al., 2024), similar elements were detected.

As presented in Fig. 2(e), the saturation magnetizations for β-CD-TA-MKL and β-CD-MA-MKL are 3.78 and 8.43 emu.g^{-1}, respectively, while β-CD-CA-MKL exhibits a saturation magnetization of 2.52 emu.g^{-1} (Sabzevar et al., 2024). Therefore, β-CD-MA-MKL exhibits better magnetic properties. According to the EDS results (Table S5), the non-magnetic organic content (carbon and oxygen) is the lowest in β-CD-MA-MKL and the highest in β-CD-CA-MKL (Sabzevar et al., 2024). The non-magnetic nature of the coating reduces the saturation magnetization of Fe_3O_4 nanoparticles; thicker coatings increase their dipole moment while decreasing effective magnetic content, thereby diminishing overall magnetic performance (Cao et al., 2023). This trend is consistent with previous reports (Petrie et al., 2021; Zhou et al., 2021). Therefore, there is a clear correlation between the amount of inorganic fraction and magnetic properties; Increasing organic content causes a decrease in saturation magnetization. Additionally, based on the results of this study, the extent of the decrease in saturation magnetization may depend on the spatial arrangement of the cross-linkers and the placement of the organic part relative to the magnetic lignin nanoparticles within the adsorbent structure. Despite the relatively low magnetization values, these adsorbents demonstrate efficient separation from aqueous media, consistent with findings by Liu et al. (2024).

The charge properties of the adsorbents were analyzed to assess the impact of different cross-linkers on their surface characteristics. This evaluation involved measuring the zeta potential (Fig. S4) of the adsorbents as a key indicator influencing electrostatic interactions (Song et al., 2024). The adsorbents exhibited similar zeta potential profiles, showing a negative charge across a pH range of 3–11, indicating a reduced protonation of the functional groups on their surfaces (Jiang et al., 2021). However, β-CD-TA-MKL displayed the most negative zeta potential, which may be attributed to its higher content of oxygen-containing functional groups on the surface (Ahmad et al., 2019). In contrast, β-CD-CA-MKL (Sabzevar et al., 2024) and β-CD-MA-MKL exhibited less negative zeta potentials.

Based on the superior performance of β-CD-TA-MKL in the removal of MB, XPS analysis was conducted for this adsorbent. The XPS spectra of β-CD-TA-MKL are shown in Fig. S5(a). The spectra reveal peaks at 710.86, 531.42, and 284.69 eV for Fe 2p, O 1s, and C1 s, respectively. Compared to MKL (Sabzevar et al., 2024), incorporating β-CD onto MKL enhances the intensity of the C1 s and O1 s peaks in β-CD-TA-MKL. The results of the atomic composition of the β-CD-TA-MKL are given in Table S6. Additional XPS details are provided in the SI (Section S-6, Fig. S5(b–d)).

3.3. Adsorption performance

The experimental design and the associated response values are presented in Table S7. The experimental data were analyzed using linear, quadratic, and cubic models, showing that the quadratic model was highly significant and suitable for representing the response in MB dye removal. A quadratic polynomial model provides the best fit to the experimental data, as shown in Eq. (1).

$$\text{Sqrt (Adsorption capacity)} = 6.74 + 0.1334 \times A - 0.8448 \times B + 0.0333 \times C - 0.0440 \times AB - 0.0344 \times A^2 + 0.1647 \times B^2 \tag{1}$$

The significance and adequacy of the models were evaluated using ANOVA (Kumari et al., 2022), with the results summarized in Table S8. Previous studies have emphasized that a high *F*-value and a low *p*-value (<0.05) indicate a more significant impact of the variable (Kumari et al., 2024a; Moatamed Sabzevar and Ghahramaninezhad, 2024). The *F*-value for the quadratic model regression is 2240.99, with a very low *p*-value (<0.0001), indicating the statistical significance of the quadratic model. The lack of fit was also assessed relative to pure error. A significant lack of fit (*p*-value < 0.05) suggests that the model does not align well with the experimental data, potentially leading to unreliable predictions.

In contrast, a non-significant lack of fit (*p*-value > 0.05) indicates that the model fits well with the experimental data and that the variables have a meaningful impact on the model (Adamu et al., 2022). In this study, the lack-of-fit value of 0.9327 is not significant compared to pure error, indicating the adequacy of the model. Other parameters, such as the coefficient of determination (R^2), adjusted R^2 (R^2_{adj}), predicted R^2 (R^2_{pred}), and the coefficient of variation (CV%), were employed to evaluate the effectiveness of the developed model. A high R^2 value, close to 1.0, suggests strong predictive efficiency in a model (Kumari and Gupta, 2019). The proposed model has an exceptionally high R^2 value of 0.9980, indicating that the regression model explains almost all the variation in the data, leaving only 0.6286 % unexplained. Furthermore, the close alignment between the R^2_{adj} (0.9976) and R^2_{pred} (0.9967) values further supports the model's reliability and significance. The discrepancy between R^2_{adj} and R^2_{pred} should ideally be less than 0.20; if the difference exceeds 0.20, the model is considered unsuitable for the data (Adamu et al., 2022). The standard deviation derived from the software
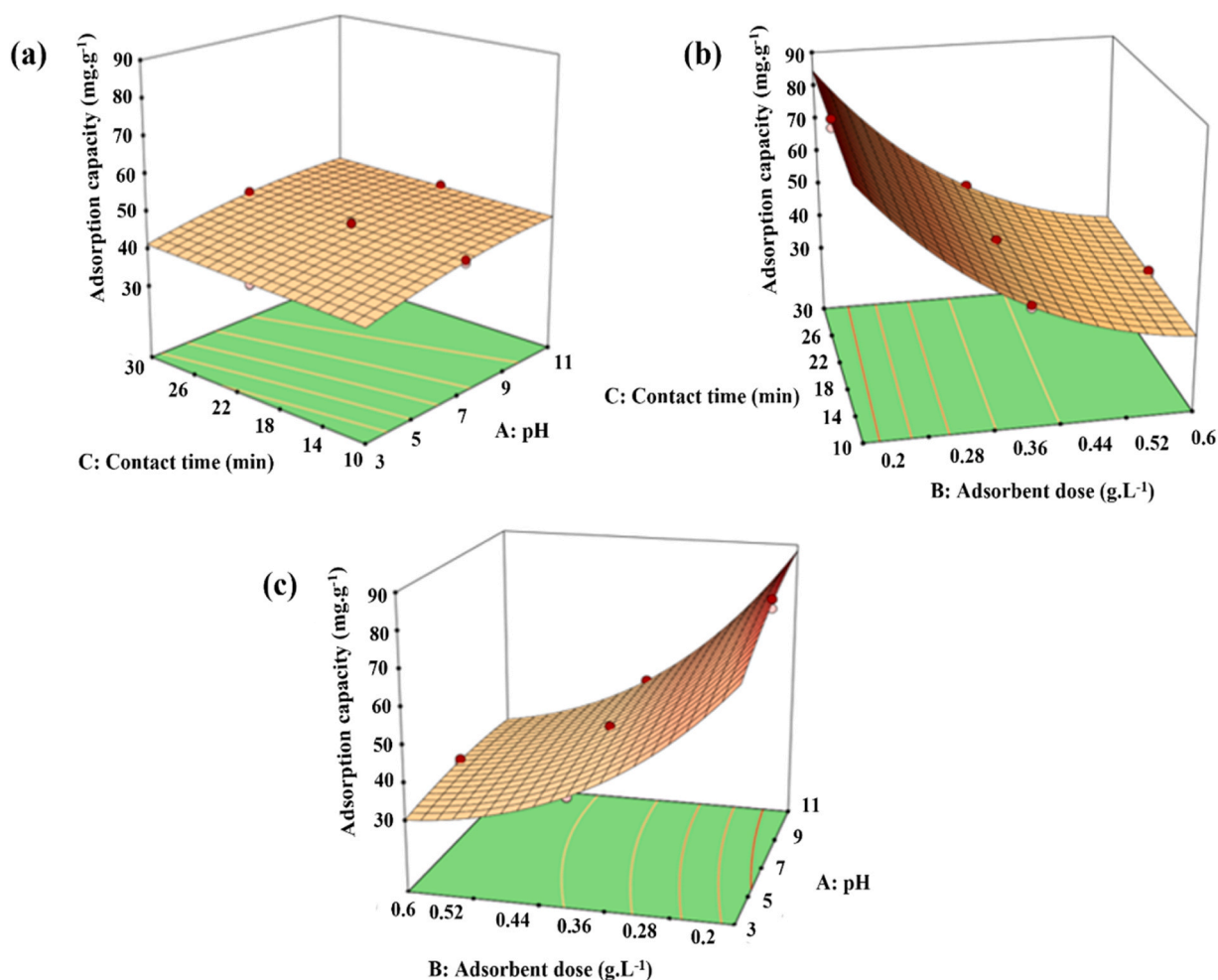

Fig. 3. Surface plots of (a) pH and contact time, (b) adsorbent dose and contact time, and (c) pH and adsorbent dose.

output was 0.0432. Small standard deviation values in relation to the model means provided additional evidence of the models' accuracy and predictive adequacy (Adamu et al., 2022).

Adequate Precision (Adeq Precision) determines the signal-to-noise ratio; a desirable ratio should be greater than 4 (Sabzevar et al., 2025). In this study, the Adeq Precision of the model was 172.55, indicating a strong signal for exploring the design space (Kumari and Gupta, 2019). Additionally, the p-values for pH (A), adsorbent dose (B), and contact time values (C) were all below 0.05, highlighting their statistical significance. These findings confirm that the three factors significantly influenced MB removal. As shown in Table S8, higher F-values indicate a greater impact and statistical significance in the removal process.

The residuals in the normal probability plot (Fig. S6(a)) form a fairly straight line and indicate that the errors follow a normal distribution (Alam et al., 2022). Residuals represent the differences between experimental and predicted data (Deymeh et al., 2024). Low residual values suggest that the model predictions are highly accurate. The plot of predicted versus actual values in Fig. S6(b) reveals a strong correlation between the adsorption values, emphasizing the high accuracy of the model (Hamouda et al., 2020). These findings confirm that the model effectively represents the experimental data and can be considered a reliable correlation model. Three-dimensional (3D) response surface plots were utilized to examine the interactions between pH, adsorbent dose, and contact time values. Fig. 3(a) illustrates the interaction between contact times (10–30 min) and pH (3−11). pH is one of the key factors affecting the adsorption process. At constant contact time, as pH increases from 3–11, the adsorption capacity of MB improves. The interaction between the dye molecules and the adsorbent is primarily driven by electrostatic forces, with the negatively charged hydroxyl and carboxyl groups on the adsorbent attracting the positively charged MB dye in water (Omwoyo and Otieno, 2024). Additionally, under acidic conditions, the concentration of hydrogen ions in the solution rises, competing with MB for adsorption sites and further decreasing MB removal efficiency (Buenaño et al., 2024).

This finding is consistent with the results reported by Alam et al., where increased solution pH positively influences MB removal (Alam et al., 2022) and adsorption capacity. The time required for contact between the adsorbent and adsorbate is essential in adsorption studies. The findings of this study (Fig. 3(a)) show that as contact time increases, the adsorption capacity of MB also rises. Extended contact allows more interactions between the dye molecules and the adsorbent surface. Initially, the adsorption capacity increases with time, but eventually, it reaches a relatively stable level, indicating equilibrium. The early increase in adsorption rate is attributed to the higher availability of active sites during the initial stages (Buenaño et al., 2024). The maximum adsorption capacity was achieved at a pH of 11 and a contact time of 30 min.

The effect of the adsorbent dose (0.2–0.6 g.L^{-1}) and contact time (10–30 min) on MB removal was investigated, with the interaction plot shown in Fig. 3(b). At a specific time, the inverse relationship between adsorption capacity and adsorbent dose can be attributed to the high affinity between adsorbate molecules and adsorbent sites at an initially low dose (0.2 g.L^{-1}). From 0.2–0.6 g.L^{-1}, the sorption capacity drops as the adsorbent dose rises. Although the number of available sorption sites has increased, this decrease is probably the result of adsorbent particle aggregation, active site blockage, and decreased accessibility to active sites. Similar findings from earlier research have indicated that adsorption capacity decreases as the adsorbent dose increases (Aniagor et al., 2021). As shown in Fig. 3(c) and supported by the statistical results in Table S8, the interaction between adsorbent dose and pH was statistically significant. A visual representation indicates that adsorption capacity increases with rising pH and decreasing adsorbent dose. Under an initial dye concentration of 20 mg.L^{-1}, a solution pH of 11, 0.2 g.L^{-1} of adsorbent, and a contact time of 30 min, the highest MB adsorption capacity was achieved.

The desirability function, which ranges from 0 (undesirable) to 1 (desirable), directed the optimization process to maximize desirability (Hamouda et al., 2020). Through numerical optimization, the conditions that maximize the desirability function were identified. The highest desirability ratio of 0.974 corresponded to optimal conditions: an adsorbent dose of approximately 0.2 g.L^{-1}, pH 11, and a contact time of 30 min. Under these settings, the maximum removal efficiency and adsorption capacity achieved were 97.32% and 83.76 mg.g^{-1}, respectively, demonstrating the high efficacy of the optimized parameters for MB removal. Two additional tests were performed under the same conditions to validate the accuracy of the model. The results showed MB removal efficiencies of 96.24% and 95.10% and adsorption capacities of 83.26 mg g^{-1} and 82.27 mg.g^{-1}, respectively (Table S9). These experimental values closely matched the predicted values, indicating the model's high accuracy and reliability. This agreement between the observed and predicted values shows the accuracy and reliability of the model. Consequently, the model can be considered a reliable tool for predicting and enhancing the effectiveness of MB removal and adsorption capacity in practical scenarios.

To evaluate the adsorbent's performance under more practical conditions, re-optimization was carried out at a neutral pH (pH 7). Under these conditions, a removal efficiency of 91.5 % and an adsorption capacity of 81.27 mg.g^{-1} were achieved using the same adsorbent dose (0.005 g in 25 mL) and contact time (30 min). These findings suggest that the adsorbent can be utilized in industrial applications, as it remains effective at neutral pH levels.

3.4. Evaluation of kinetic models in the adsorption process

To evaluate the adsorption rate, kinetic experiments were carried out by observing changes in the adsorption capacity of β-CD-TA-MKL over time. Specifically, 0.005 g of β-CD-TA-MKL was added to 25 mL of MB solutions with initial concentrations of 20 and 40 mg.L^{-1} at pH 11.

The adsorption capacity of β-CD-TA-MKL was evaluated as a function of contact time (10–30 min). Equilibrium for MB adsorption was reached at approximately 30 min, with high removal efficiencies of 96.85 % and 81.37 % and corresponding adsorption capacities of 84.14 and 158.84 mg.g^{-1} for initial MB concentrations of 20 and 40 mg.L^{-1}, respectively. To investigate the adsorption kinetics and underlying mechanism, two linear kinetic models, the pseudo-first-order (PFO) and pseudo-second-order (PSO) models (Sabzevar et al., 2024), were applied. The resulting fitting parameters are presented in Fig. S7(a) and Table S10. Based on the R^2 values close to

unity, the PSO model provided a better fit than the PFO model. Furthermore, the experimentally observed adsorption capacity ($q_{e,exp}$) closely matched the value calculated ($q_{e,cal}$) from the PSO model, indicating that the PSO model is more applicable for describing dye removal from aqueous solutions. A more detailed analysis based on statistical indices (Table S10) showed that the PSO model, with its lower error values, provides a superior description of the kinetic results. These observations are consistent with those reported by Hu et al. (Hu et al., 2023) and El Haddad (El Haddad, 2016). Fig. S7(b) shows the results of fitting the experimental data to the PSO model for initial concentrations of 20 and 40 mg.L^{-1}.

3.5. Evaluation of isotherm models in the adsorption process

Adsorption isotherms represent the interaction between the adsorbent and adsorbate during the adsorption process (Takabi et al., 2021). Therefore, it is important to study the isotherm data to develop an equation that can describe the results and be utilized for design (Kumari et al., 2023a). The adsorption values were analyzed using two fundamental isotherm models, Langmuir and Freundlich, as described by Eqs. (S10) and (S11) (Section S-7). In the Langmuir model, the dimensionless parameter R_L was used to check the suitability of the adsorbent for MB dye, which was calculated using Eq. (S12) (Section S-7).

Fig. S7(c) shows the linear fitting plots for the Langmuir and Freundlich models, with the corresponding isotherm parameters detailed in Table S11. The results indicate that the Langmuir model with a relatively higher R^2 value provides a better fit to the equilibrium data, suggesting a monolayer adsorption process (Khoshkho et al., 2021) of MB onto β-CD-TA-MKL. In addition, the Langmuir model, which had the lowest statistical indices, was more satisfactory in explaining the adsorption behavior compared to the Freundlich model (El Haddad, 2016; Hu et al., 2023).

The R_L values in Table S11 ($0 < R_L < 1$) suggest that the adsorption of MB on the adsorbent surface is favorable, indicating a relatively strong interaction between the dye molecules and the adsorbent. Additionally, the Freundlich isotherm parameter, n, ranging from 2 to 10, supports the conclusion that the adsorption process is favorable. The rise in the K_F value with increasing temperature indicates improved adsorption efficiency at higher temperatures (Ahmadpour et al., 2023). Moreover, the adsorption capacity of β-CD-TA-MKL was observed to increase with temperature. As the temperature rose from 298 to 318 K, the adsorption capacity increased from 384.61 to 454.54 mg.g^{-1}, indicating an endothermic adsorption process (Jemli et al., 2024).

A comparative analysis with other adsorbents reported in the literature is provided in Table S12, highlighting the potential of β-CD-TA-MKL for MB adsorption. Among the adsorbents reviewed, β-CD-TA-MKL exhibits a notably high adsorption capacity. The developed adsorbent makes it a promising candidate for MB adsorption from contaminated water in industrial applications.

3.6. Adsorption thermodynamics

Thermodynamic studies of MB adsorption on β-CD-TA-MKL at various temperatures (298–318 K) were conducted. The thermodynamic parameters of the adsorption process were determined using Eqs. (S13) to (S15) in Section S-8. The standard Gibbs free energy change values (ΔG°) were obtained -28.29, -30.19, and -32.28 kJ.mol^{-1} for 298, 308, and 318 K temperatures, respectively. Moreover, the positive enthalpy value (ΔH°, 31.13 kJ.mol^{-1}) suggests that the adsorption is endothermic, consistent with experimental observations that show MB adsorption capacity increases with rising temperature. ΔH° values below 80 kJ.mol^{-1} imply physical adsorption (Tran, 2022). Nonetheless, chemical adsorption appears to be the predominant process based on the high agreement between the experimental data and the PSO kinetic model (Wei et al., 2023). Consequently, it appears that both chemical and physical interactions have an impact on the adsorption. Previous research has documented similar differences between thermodynamic and kinetic interpretations (Tran, 2022), underscoring the need to consider both thermodynamic and kinetic factors for a complete understanding of the adsorption process.

The positive entropy (ΔS°, 199.30 J.mol^{-1}.K^{-1}) indicates a strong affinity of the adsorbent for MB molecules, likely due to bond disruption between the dye and water molecules as well as increased molecular randomness at the solid-solution interface during adsorption (Ahmadpour et al., 2023).

3.7. Regeneration and reusability of adsorbent

Adsorbents used for industrial water remediation must be stable, making the regeneration ability of adsorbents crucial for their practical applications (Jia et al., 2024). The regeneration process depends on adsorbate concentration and the forces between the adsorbate and adsorbent material (Kumari et al., 2024b). The reusability of the β-CD-TA-MKL bio-adsorbent was examined to evaluate its potential for practical dye removal from wastewater. In each cycle, 0.005 g of adsorbent was mixed with an MB solution (20 mg. L^{-1}) for 30 min to achieve complete adsorption. Desorption was performed using a 3:1 mixture of ethanol and 0.1 M HCl for 30 min. Dye removal efficiency for β-CD-TA-MKL declined from 96.24±0.67% to 91.10±1.13% after five cycles (Fig. S8(a)), and statistical details regarding the standard deviation for each cycle are shown in Table S13. This decrease in adsorption efficiency is likely due to the saturation of the adsorbent sites with MB molecules after each cycle, resulting in fewer available sites for subsequent adsorption. After the fifth recovery, the recycled adsorbent was analyzed using characterization techniques, FT-IR, and VSM. The FT-IR spectrum of the recovered β-CD-TA-MKL shows the same characteristic peaks as the fresh adsorbent (Fig. S8(b)). However, a slight reduction in the intensity of β-CD peaks at 3408, 1747, 1633, and 1035 cm^{-1} was observed. This reduction may result from factors such as the recycling process and drying conditions, which could introduce structural defects in the surface layer, thereby diminishing the intensity of these peaks (Liu, Z. et al., 2024). Since no notable variation was detected in the percentage of removal, and peaks related to the functional groups did not change after the fifth recovery, we believe that this decrease in the intensity of the peaks is due to the

places that are still involved in pollutant molecules, and they have not been completely removed. Furthermore, the saturation magnetic strength of β-CD-TA-MKL remained relatively stable, decreasing slightly from 3.78 to 3.38 emu.g^{-1} post-recycling (Fig. S8(c)).

According to the recovery results and analyses performed on the adsorbent after the fifth cycle, it shows favorable stability and recyclability for practical applications. Similar results have been reported for β-CD-containing adsorbents, where the removal efficiency decreased only slightly after several recovery cycles (Li et al., 2022; Singh et al., 2024; Verma et al., 2022; Yang et al., 2021).

3.8. Effect of competitive ion (NaCl) on MB removal

To better replicate real environmental co-adsorption scenarios, the impact of NaCl concentration on the removal of MB was investigated. Fig. S8(d) and Table S14 show that the amount of dye adsorbed on β-CD-TA-MKL decreased with increasing NaCl concentration. This reduction is likely because of competition between Na⁺/Cl⁻ ions and MB molecules for the available active sites (Imessaoudene et al., 2022). Similar results were also reported by Yagub et al. (Yagub et al., 2014) and Imessaoudene et al. (Imessaoudene et al., 2022). Details on adsorbent selectivity (Section S-9) and statistical details regarding the standard deviation are provided in the SI, while the corresponding error bars are shown in Fig. S9.

3.9. Mechanism of adsorption

The exceptional efficiency of β-CD-TA-MKL in the removal of MB is attributed to its unique structure and diverse functional groups. A systematic approach was employed to elucidate the key mechanisms underlying the adsorption process, as outlined in Fig. 4. The well-organized structure of β-CD-TA-MKL and its high adsorption performance are attributed to the synergistic effects between MKL, TA, and β-CD. To further validate the adsorption mechanism, FTIR analysis of β-CD-TA-MKL was performed before and after MB adsorption, revealing important insights into changes in functional groups and shedding light on the adsorption mechanism.

In Fig. S10, the peak of the adsorbent at 3408 cm^{-1} changed to 3427 cm^{-1} and became less intense after adsorption. This suggests that the adsorption process affects the hydroxyl groups in the adsorbent (Lagiewka et al., 2023). The decrease in peak intensity and shift of the C-H stretching vibration from 2928 cm^{-1} to 2927 cm^{-1} indicate a hydrophobic interaction between the adsorbent and the adsorbate (Wei et al., 2023). The peak intensity at 1747 cm^{-1} in spectra (A) notably decreases, and a peak moves a little after adsorption, indicating an interaction between the C=O group of the cross-linker and cationic molecules of dye (Sharma and Das,
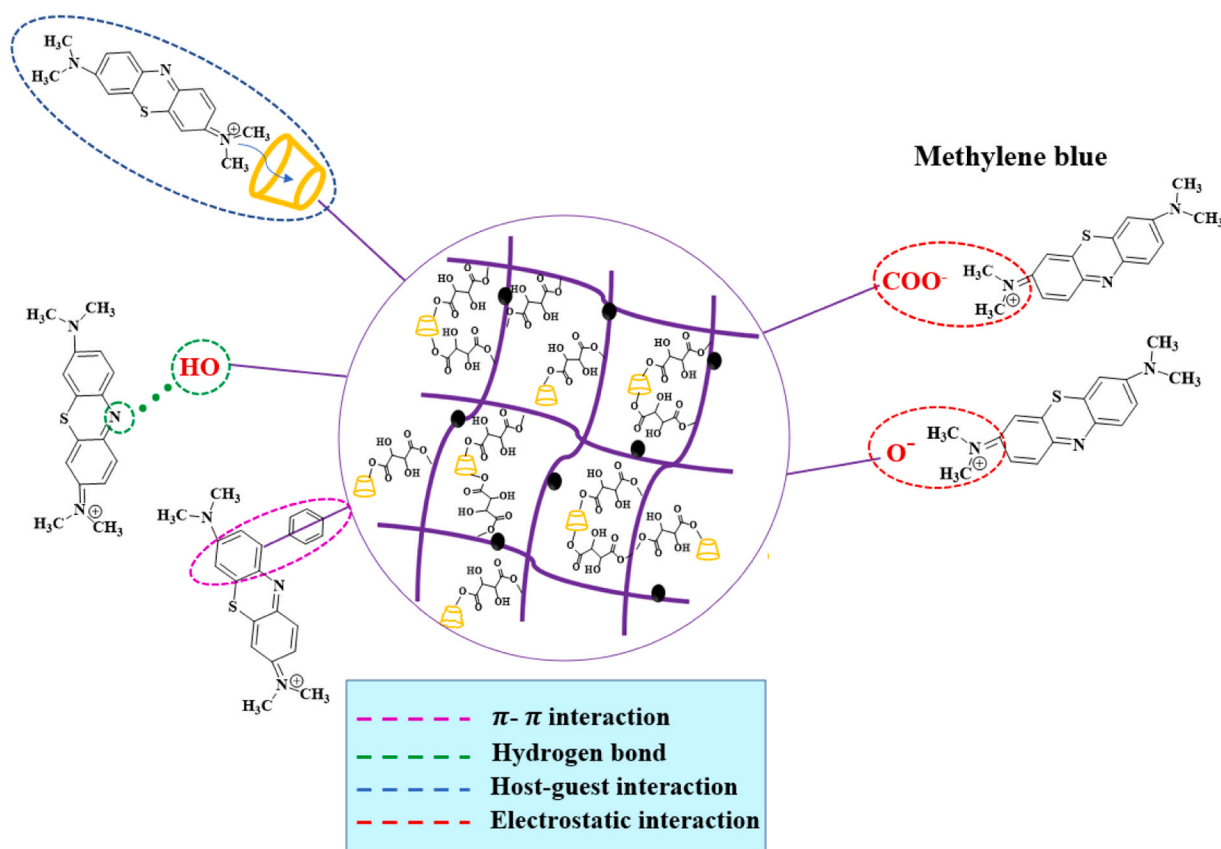

Fig. 4. Mechanism of MB adsorption onto β-CD-TA-MKL.

2013). The peak located at 1633 cm^{-1}, belonging to C-C in the spectrum (A), is shifted to 1599 cm^{-1} in spectra (B), suggesting a π-π interaction between the adsorbent and pollutant (Wei et al., 2023). After adsorption, the reduced intensity of the peak at 1035 cm^{-1} and its shift to 1027 cm^{-1} suggest interactions between β-CD glucose rings and MB, indicating that dye molecules may be inserted into the cyclodextrin cavities (Qin et al., 2019).

The MB sorption mechanism on β-CD-TA-MKL involves four types of interactions: hydrogen bonding, electrostatic interactions, host-guest interactions, and π-π interaction. Compared to MKL, β-CD-TA-MKL contains more oxygen-containing groups, contributing to its superior adsorption performance. These additional oxygen groups provide more active sites, enhancing interactions with MB and increasing its adsorption capacity. The -OH groups in β-CD-TA-MKL serve as hydrogen bond donors, facilitating interactions with dye molecules. The electrostatic interactions play a key role in cationic dye sorption. The -OH and -COOH groups on the sorbent can ionize in aqueous environments, creating negatively charged sites on the sorbent's surface (Rohith and Girija, 2024). The π-π interaction also arises from the aromatic structures in the dye molecules and β-CD-TA-MKL. Specifically, the aromatic rings in β-CD-TA-MKL interact with the π-electrons of the dye molecules' aromatic rings. Additionally, the β-CD component of the sorbent contains macromolecular cavities that facilitate the formation of inclusion complexes with guest molecules, further enhancing the sorption process (Rohith and Girija, 2024).

3.10. Limitations and future work

Although the synthesis conditions have been optimized to enhance the adsorbent's performance for MB removal, several limitations remain, including the need for further optimization of the adsorbent to evaluate its performance in complex wastewater matrices with multiple competing pollutants. Future research can overcome these limitations by investigating the adsorbent's performance in a broader range of contaminants and real wastewater matrices, enhancing its scalability, and evaluating its stability and selectivity for other pollutants.

Details on economic and environmental aspects are given in Section S-10.

4. Conclusions

This work evaluates the effect of environmentally friendly cross-linkers (citric acid, malic acid, and tartaric acid) on the performance of adsorbents for cationic dye removal. Analytical techniques were employed to verify the successful synthesis of adsorbents. The performance evaluation of the synthesized adsorbents revealed that the presence of tartaric acid as a cross-linker in the adsorbent, consisting of magnetic lignin and beta-cyclodextrin, exhibited superior performance compared to those containing malic acid and citric acid, confirming our hypothesis. The optimal conditions for methylene blue removal (∼97%) were determined using Design Expert software. These conditions included a contact time of 30 min, a pH of 11, and a dose of 0.2 g.L^{-1}. The adsorption process followed pseudo-second-order kinetics and conformed to the Langmuir isotherm model. Thermodynamic analysis showed that the adsorption process was endothermic. The β-CD-TA-MKL adsorbent showed excellent stability and reusability. These findings highlight the potential of β-CD-TA-MKL as an efficient adsorbent for industrial applications.

CRediT authorship contribution statement

Arash Arami-Niya: Writing – review & editing, Validation, Project administration, Conceptualization. **Ali Ahmadpour:** Writing – review & editing, Validation, Supervision, Methodology, Funding acquisition, Data curation, Conceptualization. **Mahboube Ghahramaninezhad:** Writing – review & editing, Validation, Project administration, Methodology, Conceptualization. **Arefe Moatamed Sabzevar:** Writing – review & editing, Writing – original draft, Visualization, Methodology, Investigation, Formal analysis, Conceptualization.

Declaration of Competing Interest

The authors declare that they have no known competing financial interests or personal relationships that could have appeared to influence the work reported in this paper.

Acknowledgments

Appendix A. Supporting information

Supplementary data associated with this article can be found in the online version at doi:10.1016/j.eti.2025.104507.

Data availability

Data will be made available on request.

References

Adamu, M., Marouf, M.L., Ibrahim, Y.E., Ahmed, O.S., Alanazi, H., Marouf, A.L., 2022. Modeling and optimization of the mechanical properties of date fiber reinforced concrete containing silica fume using response surface methodology. Case Stud. Constr. Mater. 17, e01633.

Ahmad, S., Ahmad, A., Khan, S., Ahmad, S., Khan, I., Zada, S., Fu, P., 2019. Algal extracts based biogenic synthesis of reduced graphene oxides (rGO) with enhanced heavy metals adsorption capability. J. Ind. Eng. Chem. 72, 117–124.

Ahmadpour, A., Tanhaei, B., Khoshkho, S.M., Ayati, A., Krivoshapkin, P., Sillanpää, M., 2023. Dual-purpose magnetic κ-carrageenan/montmorillonite hydrogel for carrying and removal of tetracycline from aqueous medium. Inorg. Chem. Commun. 156, 111274.

Alam, M.Z., Bari, M.N., Kawsari, S., 2022. Statistical optimization of methylene blue dye removal from a synthetic textile wastewater using indigenous adsorbents. Environ. Sustain. Indic. 14, 100176.

Altayan, M.M., Tzoupanos, N., Barjenbruch, M., 2023. Polymer based on beta-cyclodextrin for the removal of bisphenol A, methylene blue and lead (II): preparation, characterization, and investigation of adsorption capacity. J. Mol. Liq. 390, 122822.

Aniagor, C.O., Elshkankery, M., Fletcher, A., Morsy, O.M., Abdel-Halim, E., Hashem, A., 2021. Equilibrium and kinetic modelling of aqueous cadmium ion and activated carbon adsorption system. Water Conserv. Sci. Eng. 6 (2), 95–104.

Buenaño, L., Ali, E., Jafer, A., Zaki, S.H., Hammady, F.J., Khayoun Alsaadi, S.B., Karim, M.M., Ramadan, M.F., Omran, A.A., Alawadi, A., 2024. Optimization by Box–Behnken design for environmental contaminants removal using magnetic nanocomposite. Sci. Rep. 14 (1), 6950.

Cao, L.N.H., Luong, H.V.T., Dang, H.G., Ho, Q.P., Vo, T.N.Y., Dang, T.V.A., 2023. Preparation and characterization of magnetic-lignin nanoparticles with potential applications for drug delivery. CTU J. Innov. Sustain. Dev. 15 (3), 64–71.

Castro, D.P.D., Santana, R.M.C., 2024. Influence of chemical nature of citric and tartaric acids on reaction time of the crosslinking of polyvinyl alcohol hydrogels. An. da Acad. Bras. De. Ciências 96 (1), e20230092.

Chahal, M., Kumari, S., Bhattacharya, A., Garg, M.C., 2024. Evaluating sustainable agricultural waste biomass for methylene blue adsorption in wastewater treatment: a state-of-the-art review. Bioresour. Technol. Rep. 28, 101983.

Deymeh, F., Ahmadpour, A., Allahresani, A., Arami-Niya, A., 2024. Collaborative adsorption and photocatalytic degradation of high concentration pharmaceutical pollutants in water using a novel dendritic fibrous nano-silica modified with chitosan and UiO-66. Int. J. Biol. Macromol. 275, 133534.

El Haddad, M., 2016. Removal of basic fuchsin dye from water using mussel shell biomass waste as an adsorbent: equilibrium, kinetics, and thermodynamics. J. Taibah Univ. Sci. 10 (5), 664–674.

El-Tahlawy, K., Gaffar, M.A., El-Rafie, S., 2006. Novel method for preparation of β-cyclodextrin/grafted chitosan and it's application. Carbohydr. Polym. 63 (3), 385–392.

Ghahramaninezhad, M., Ahmadpour, A., 2022. Carboxylmethyl-β-cyclodextrin as a good modifier agent for oxidation of dibenzothiophene. Surf. Interfaces 28, 101612.

Ghorpade, V.S., Yadav, A.V., Dias, R.J., 2016. Citric acid crosslinked cyclodextrin/hydroxypropylmethylcellulose hydrogel films for hydrophobic drug delivery. Int. J. Biol. Macromol. 93, 75–86.

Hamouda, R.A., El-Naggar, N.E.-A., Doleib, N.M., Saddiq, A.A., 2020. Bioprocessing strategies for cost-effective simultaneous removal of chromium and malachite Green by marine alga enteromorpha intestinalis. Sci. Rep. 10 (1), 13479.

Hu, Q.-D., Jiang, H.-L., Lam, K.-H., Hu, Z.-P., Liu, Z.-J., Wang, H.-Y., Yang, Y.-Y., Baigenzhenov, O., Hosseini-Bandegharaei, A., He, F.-A., 2023. Polydopamine-modification of a magnetic composite constructed from citric acid–cross-linked cyclodextrin and graphene oxide for dye removal from waters. Environ. Sci. Pollut. Res. 30 (32), 78521–78536.

Imessaoudene, A., Cheikh, S., Bollinger, J.-C., Belkhiri, L., Tiri, A., Bouzaza, A., El Jery, A., Assadi, A., Amrane, A., Mouni, L., 2022. Zeolite waste characterization and use as low-cost, ecofriendly, and sustainable material for malachite Green and methylene blue dyes removal: Box–behnken design, kinetics, and thermodynamics. Appl. Sci. 12 (15), 7587.

Jemli, S., Lütke, S.F., Chamtouri, F., Amara, F.B., Bejar, S., Oliveira, M.L.S., Knani, S., Silva, L.F.O., Dotto, G.L., 2024. A novel cartoon crosslinked β-cyclodextrin (C-β-CD) polymer for effective uptake of hg from aqueous solutions: kinetics, equilibrium, thermodynamics, and statistical physics approach. Sep. Purif. Technol. 330, 125578.

Jia, J., Wu, D., Yu, J., Gao, T., Guo, L., Li, F., 2024. Upgraded β-cyclodextrin-based broad-spectrum adsorbents with enhanced antibacterial property for high-efficient dyeing wastewater remediation. J. Hazard. Mater. 461, 132610.

Jiang, L.-W., Zeng, F.-T., Zhang, Y., Xu, M.-Y., Xie, Z.-W., Wang, H.-Y., Wu, Y.-X., He, F.-A., Jiang, H.-L., 2021. Preparation of a novel Fe3O4/graphite oxide nanosheet/citric acid-crosslinked β-cyclodextrin polymer composite to remove methylene blue from water. Adv. Powder Technol. 32 (2), 492–503.

Khoshkho, S.M., Tanhaei, B., Ayati, A., Kazemi, M., 2021. Preparation and characterization of ionic and non-ionic surfactants impregnated κ-carrageenan hydrogel beads for investigation of the adsorptive mechanism of cationic dye to develop for biomedical applications. J. Mol. Liq. 324, 115118.

Kumari, S., Agrawal, N.K., Agarwal, A., Kumar, A., Malik, K., Goyal, D., Rajput, V.D., Minkina, T., Sharma, P., Garg, M.C., 2023a. A prominent streptomyces sp. Biomass-based biosorption of zinc (II) and lead (II) from aqueous solutions: isotherm and kinetic. Separations 10 (7), 393.

Kumari, S., Chowdhry, J., Choudhury, A., Agarwal, S., Narad, P., Garg, M.C., 2024a. Machine learning approaches for the treatment of textile wastewater using sugarcane bagasse (Saccharum officinarum) biochar. Environ. Sci. Pollut. Res. 1–19.

Kumari, S., Chowdhry, J., Kumar, M., Garg, M.C., 2024b. Machine learning (ML): an emerging tool to access the production and application of biochar in the treatment of contaminated water and wastewater. Groundw. Sustain. Dev. 26, 101243.

Kumari, S., Chowdhry, J., Sharma, P., Agarwal, S., Garg, M.C., 2023b. Integrating artificial neural networks and response surface methodology for predictive modeling and mechanistic insights into the detoxification of hazardous MB and CV dyes using saccharum officinarum L. Biomass. Chemosphere 344, 140262.

Kumari, M., Gupta, S.K., 2019. Response surface methodological (RSM) approach for optimizing the removal of trihalomethanes (THMs) and its precursor's by surfactant modified magnetic nanoadsorbents (sMNP)-An endeavor to diminish probable cancer risk. Sci. Rep. 9 (1), 18339.

Kumari, S., Rajput, V.D., Minkina, T., Rajput, P., Sharma, P., Verma, A.K., Agarwal, S., Garg, M.C., 2022. Application of RSM for bioremoval of methylene blue dye from industrial wastewater onto sustainable walnut shell (Juglans regia) biomass. Water 14 (22), 3651.

Kumari, S., Singh, S, Lo, S.-L., Sharma, P., Agarwal, S., Garg, M.C., 2025. Machine learning and modelling approach for removing methylene blue from aqueous solutions: optimization, kinetics and thermodynamics studies. J. Taiwan Inst. Chem. Eng. 166, 105361.

Kwak, S., 2023. Are only p-values less than 0.05 significant? A p-value greater than 0.05 is also significant! J. Lipid Atheroscler. 12 (2), 89.

Lagiewka, J., Nowik-Zajac, A., Pajdak, A., Zawierucha, I., 2023. A novel multifunctional β-cyclodextrin polymer as a promising sorbent for rapid removal of methylene blue from aqueous solutions. Carbohydr. Polym. 307, 120615.

Li, T., Tong, Z., Zheng, Q., Bao, H., Partow, A., Meng, S., Li, L., Li, Y.C., 2021. Fabrication of a lignin-based magnetic nanocomposite adsorbent to recover phosphorus in water for agricultural reuse. ACS Sustain. Chem. Eng. 9 (31), 10468–10478.

Li, Y., Yu, E., Sun, S., Liu, W., Hu, R., Xu, L., 2022. Fast and highly efficient adsorption of cationic dyes by phytic acid crosslinked β-cyclodextrin. Carbohydr. Polym. 284, 119231.

Liu, D., Huang, Z., Li, M., Sun, P., Yu, T., Zhou, L., 2019. Novel porous magnetic nanospheres functionalized by β-cyclodextrin polymer and its application in organic pollutants from aqueous solution. Environ. Pollut. 250, 639–649.

Liu, Z.-J., Jiang, H.-L., Xiao, J.-W., Lv, H.-W., He, F.-A., Xu, J.-S., Hu, Q.-D., Zeng, F.-T., Lima, E.C., Hosseini-Bandegharaei, A., 2024. A novel aminated Fe3O4/GO/carboxylated cross-linked β-CDP composite for effective sorption of cationic and anionic dyes from water. J. Ind. Eng. Chem.

Liu, Q., Wang, J., Duan, C., Wang, T., Zhou, Y., 2022. A novel cationic graphene modified cyclodextrin adsorbent with enhanced removal performance of organic micropollutants and high antibacterial activity. J. Hazard. Mater. 426, 128074.

Liu, Z., Wang, G., Li, Y., Li, H., Deng, N., 2024. Carboxymethyl-β-cyclodextrin functionalized TiO2@ Fe3O4@ RGO magnetic photocatalyst for efficient photocatalytic degradation of tetracycline under visible light irradiation. J. Environ. Chem. Eng. 12 (5), 113303.

Moatamed Sabzevar, A., Ghahramaninezhad, M., 2024. Development of an impressive method for the synthesis of α-MoO3 nanobelts as an efficient catalyst for biodiesel production. Environ. Sci. Pollut. Res. 1–15.

Obayomi, K.S., Lau, S.Y., Danquah, M.K., Zhang, J., Chiong, T., Obayomi, O.V., Meunier, L., Rahman, M.M., 2024. A response surface methodology approach for the removal of methylene blue dye from wastewater using sustainable and cost-effective adsorbent. Process Saf. Environ. Prot. 184, 129–150.

Omwoyo, F.O., Otieno, G., 2024. Optimization of methylene blue dye adsorption onto coconut husk cellulose using response surface methodology: adsorption kinetics, isotherms and reusability studies. J. Mater. Sci. Chem. Eng. 12 (2), 1–18.

Petrie, F.A., Gorham, J.M., Busch, R.T., Leontsev, S.O., Ureña-Benavides, E.E., Vasquez, E.S., 2021. Facile fabrication and characterization of kraft lignin@ Fe3O4 nanocomposites using ph driven precipitation: effects on increasing lignin content. Int. J. Biol. Macromol. 181, 313–321.

Pooja, N., Ahmed, N.Y., Mal, S.S., Bharath, P.A.S., Zhuo, G.-Y., Noothalapati, H., Managuli, V., Mazumder, N., 2025. Assessment of biocompatibility for citric acid crosslinked starch elastomeric films in cell culture applications. Sci. Rep. 15 (1), 6427.

Qin, X., Bai, L., Tan, Y., Li, L., Song, F., Wang, Y., 2019. β-Cyclodextrin-crosslinked polymeric adsorbent for simultaneous removal and stepwise recovery of organic dyes and heavy metal ions: fabrication, performance and mechanisms. Chem. Eng. J. 372, 1007–1018.

Qu, Y., Li, H., Yakub, I., He, W., Dong, W., Barawi, M.H., Wang, S., Ma, H., Zhu, Z., 2025. Synthesis and characterization of efficient adsorbents for methylene blue based on graphene Oxide/β-cyclodextrin composites. Water Air Soil Pollut. 236 (1), 1–21.

Reza, A., Chen, L., Mao, X., 2024. Response surface methodology for process optimization in livestock wastewater treatment: a review. Heliyon 10 (9).

Rohith, M., Girija, P., 2024. Green synthesis of a multifunctional β-cyclodextrin modified polymer sorbent using agrarian wastes of nelumbo nucifera for the efficient sequestration of toxic dyes from polluted water. J. Environ. Chem. Eng. 12 (6), 114147.

Sabzevar, A.M., Ahmadpour, A., Ghahramaninezhad, M., 2024. Preparation of beta-cyclodextrin decorated magnetic lignin by citric acid cross-linker for water treatment. Carbohydr. Polym. Technol. Appl., 100654

Sabzevar, A.M., Ahmadpour, A., Ghahramaninezhad, M., Arami-Niya, A., 2025. Improving structural properties and adsorption performance of kraft lignin-based microspheres for anionic dye removal. Ind. Crops Prod. 234, 121640.

Sharma, P., Das, M.R., 2013. Removal of a cationic dye from aqueous solution using graphene oxide nanosheets: investigation of adsorption parameters. J. Chem. Eng. Data 58 (1), 151–158.

Shindhal, T., Rakholiya, P., Varjani, S., Pandey, A., Ngo, H.H., Guo, W., Ng, H.Y., Taherzadeh, M.J., 2021. A critical review on advances in the practices and perspectives for the treatment of dye industry wastewater. Bioengineered 12 (1), 70–87.

Silva, E.C., Gomes, C.G., Pina, J., Pereira, R.F., Murtinho, D., Fajardo, A.R., Valente, A.J., 2024. Carbon quantum dots-containing poly (β-cyclodextrin) for simultaneous removal and detection of metal ions from water. Carbohydr. Polym. 323, 121464.

Singh, B.K., Pande, P.P., Chaurasiya, A., Dey, K.K., Kushwaha, N., 2024. Synthesis and characterisation of novel beta-cyclodextrin based Fe3O4 nanocomposite: adsorption behaviour and photocatalytic dye degradation studies. Int. J. Environ. Anal. Chem. 1–26.

Song, S.H., Kim, C.-M., Akhte, K.M., Ishaq, A., Jee, H., Chuah, C.Y., Park, J., Chae, K.-J., Yang, E., 2024. Silver nanoparticle-decorated reduced graphene oxide/ nanocrystalline titanium metal-organic frameworks composite membranes with enhanced nanofiltration performance and photocatalytic ability. Desalin. Water Treat., 100836

Sun, Z., Feng, T., Zhou, Z., Wu, H., 2021. Removal of methylene blue in water by electrospun PAN/β-CD nanofibre membrane. ePolymers 21 (1), 398–410.

Takabi, A.S., Shirani, M., Semnani, A., 2021. Apple stem as a high performance cellulose based biosorbent for low cost and eco-friendly adsorption of crystal violet from aqueous solutions using experimental design: mechanism, kinetic and thermodynamics. Environ. Technol. Innov. 24, 101947.

Tan, Y.H., Abdullah, M.O., Nolasco-Hipolito, C., Zauzi, N.S.A., 2017. Application of RSM and taguchi methods for optimizing the transesterification of waste cooking oil catalyzed by solid ostrich and chicken-eggshell derived CaO. Renew. Energy 114, 437–447.

Tran, H.N., 2022. Is it possible to draw conclusions (adsorption is chemisorption) based on fitting between kinetic models (pseudo-second-order or elovich) and experimental data of time-dependent adsorption in solid-liquid phases? Bentham Sci. Publ. Direct 228–230.

Verma, M., Lee, I., Hong, Y., Kumar, V., Kim, H., 2022. Multifunctional β-Cyclodextrin-EDTA-Chitosan polymer adsorbent synthesis for simultaneous removal of heavy metals and organic dyes from wastewater. Environ. Pollut. 292, 118447.

Wang, H., Liu, Y.-g, Zeng, G.-m, Hu, X.-j, Hu, X., Li, T.-t, Li, H.-y, Wang, Y.-q, Jiang, L.-h, 2014. Grafting of β-cyclodextrin to magnetic graphene oxide via ethylenediamine and application for cr (VI) removal. Carbohydr. Polym. 113, 166–173.

Wei, T., Wu, H., Li, Z., 2023. Lignin immobilized cyclodextrin composite microspheres with multifunctionalized surface chemistry for non-competitive adsorption of co-existing endocrine disruptors in water. J. Hazard. Mater. 441, 129969.

Wu, H., Gong, L., Zhang, X., He, F., Li, Z., 2021. Bifunctional porous polyethyleneimine-grafted lignin microspheres for efficient adsorption of 2, 4-dichlorophe-noxyacetic acid over a wide ph range and controlled release. Chem. Eng. J. 411, 128539.

Yagub, M.T., Sen, T.K., Ang, M., 2014. Removal of cationic dye methylene blue (MB) from aqueous solution by ground raw and base modified pine cone powder. Environ. earth Sci. 71, 1507–1519.

Yang, Z., Liu, X., Liu, X., Wu, J., Zhu, X., Bai, Z., Yu, Z., 2021. Preparation of β-cyclodextrin/graphene oxide and its adsorption properties for methylene blue. Colloids Surf. B Biointerfaces 200, 111605.

Yatimzade, M.H., Ahmadpour, A., Ghahramaninezhad, M., Sabzevar, A.M., 2024. Optimizing the efficient removal of ibuprofen from water environment by magnetic carbon aerogel: kinetics, isotherms, and thermodynamic studies. J. Mol. Liq. 408, 125337.

Zhang, J., Jiang, F., Lu, Y., Wei, S., Xu, H., Zhang, J., Ge, Y., Li, Z., 2023. Lignin microparticles-reinforced cellulose filter paper for simultaneous removal of emulsified oils and dyes. Int. J. Biol. Macromol. 230, 123120.

Zhong, X., Yuan, Q., Wang, Q., Hu, C., Guo, K., Ouyang, J., Chen, M., 2022. Maleic anhydride-β-cyclodextrin functionalized magnetic nanoparticles for the removal of uranium (VI) from wastewater. Crystals 12 (12), 1731.

Zhou, Y., Hu, Y., Huang, W., Cheng, G., Cui, C., Lu, J., 2018. A novel amphoteric β-cyclodextrin-based adsorbent for simultaneous removal of cationic/anionic dyes and bisphenol a. Chem. Eng. J. 341, 47–57.

Zhou, X., Jin, C., Liu, G., Wu, G., Huo, S., Kong, Z., 2021. Functionalized lignin-based magnetic adsorbents with tunable structure for the efficient and selective removal of pb (II) from aqueous solution. Chem. Eng. J. 420, 130409.

Zhou, J., Tong, J., Su, X., Ren, L., 2016. Hydrophobic starch nanocrystals preparations through crosslinking modification using citric acid. Int. J. Biol. Macromol. 91, 1186–1193.

Zong, E., Huang, G., Liu, X., Lei, W., Jiang, S., Ma, Z., Wang, J., Song, P., 2018. A lignin-based nano-adsorbent for superfast and highly selective removal of phosphate. J. Mater. Chem. A 6 (21), 9971–9983.

Zuhara, S., Pradhan, S., Zakaria, Y., Shetty, A.R., McKay, G., 2023. Removal of methylene blue from water using magnetic GTL-derived biosolids: study of adsorption isotherms and kinetic models. Molecules 28 (3), 1511.